Anal Bioanal Chem
DOI 10.1007/s00216-010-4133-6

ORIGINAL PAPER

Fractionation and characterization of gold nanoparticles in aqueous solution: asymmetric-flow field flow fractionation with MALS, DLS, and UV–Vis detection

Tae Joon Cho · Vincent A. Hackley

Received: 9 July 2010 / Revised: 12 August 2010 / Accepted: 15 August 2010

Abstract Asymmetrical-flow field flow fractionation (AFFF) separates constituents based on hydrodynamic size and is emerging as a powerful tool for obtaining high-resolution information on the size, molecular weight, composition, and stability of nanoscale particles in liquid media. We employ a customized AFFF system combining on-line detectors for multi-angle light scattering, dynamic light scattering, and UV–Vis absorption. Our objective is to develop optimized measurement protocols for the characterization of gold nanoparticles (GNPs), which are widely utilized in biomedical research and other nanotechnology applications. Experimental conditions have been optimized by controlling key parameters, including injection volume and solids concentration, mobile phase composition, membrane type and pore size, and ratio of channel-to-cross-flow rates. Individual citrate-stabilized GNP components (nominally 10, 20, 30, 40, and 60 nm) and GNPs functionalized with polyethylene glycol were separated from multicomponent GNP mixtures by AFFF and subsequently characterized. We discuss the effects due to variations in measurement parameters and GNP surface modification on observed retention, recovery, and peak resolution.

Keywords Field flow fractionation · Gold nanoparticle · Fractionation · Size characterization · Light scattering · Particle characterization

T. J. Cho · V. A. Hackley (✉)
Materials Science and Engineering Laboratory,
National Institute of Standards and Technology,
100 Bureau Drive Stop 8520,
Gaithersburg, MD 20899-8520, USA
e-mail: vince.hackley@nist.gov

Introduction

With attributes that include chemical stability under typical biological conditions and biocompatibility, metallic gold has emerged as a material of choice for many challenging nanotechnology-based biomedical applications (e.g., drug delivery [1–5], targeted photothermal therapeutics [6–9], advanced diagnostics [10–12], and sensing devices [12–16]). The facile capacity to conjugate or functionalize gold nanoparticles (GNPs) using thiol chemistry or nonspecific interactions is a significant additional benefit, and this has allowed GNPs to be customized so as to carry targeting, imaging, and diagnostic and/or therapeutic payloads. Numerous methods now exist to produce size-controlled gold particles, ranging from small clusters containing hundreds of Au atoms [17] up to particles several hundred nanometers in diameter [18, 19]. Particle morphology can be varied from spheroidal to platelet to high-aspect rods or wires [18–22]. GNPs also exhibit strong plasmonic absorption effects [18, 19, 23], which give rise to size-specific optical properties that can be tuned for different applications. Finally, their high electron density makes them excellent markers for bio-imaging with electron microscopy [24, 25].

The in situ characterization of nanoscale objects is a considerable challenge and yet an essential component of nanotechnology development and deployment. Particle size is the principal material parameter impacting all properties of interest in nanoscale materials, although it is now widely recognized that surface chemistry can, and often does, play an equally important role. Numerous options exist for size determination in the nanoscale range, but only a subset of these approaches provide in situ analysis capability for particles in a liquid medium. Of these, only two approaches are capable of high-resolution sizing in complex multicomponent systems: centrifugation-based and chromatographic-based. Techniques

Published online: 30 August 2010

such as analytical ultracentrifugation and x-ray disc centrifugation are applicable to many relevant systems but are inflexible in adapting to different or complex material systems with challenging analytical requirements. Methods such as size exclusion chromatography (SEC) and field flow fractionation (FFF) offer more flexibility. SEC is somewhat more limited due to the interaction of the stationary phase, but is the method of choice for separation and analysis of macromolecular species. In the 1960s, the concept and theory of FFF was first proposed by Giddings [26]. FFF can be thought of as a fusion between liquid chromatography and field-driven methods like centrifugation. Furthermore, FFF has significant advantages for application to nanoscale and microscale particles, as demonstrated by the wide range of reported materials [27–30], including polymers [31–34], inorganic colloids [35], bacteria [36, 37], nucleic acids [38, 39], viruses [40, 41], and carbon nanotubes [42, 43], over a size range from 1 nm to 100 μm [44].

Different "fields" can be utilized in the application of FFF. Among these, asymmetric flow (Fig. 1a) is the most widely used [28, 44, 45], due to its experimental flexibility, simplicity, and wide compatibility with different test materials, particle size, and mobile phase compositions. Asymmetric-flow field flow fractionation (AFFF) separates constituents hydrodynamically as they migrate along a thin channel within a parabolic laminar flow profile. Onto this laminar flow, a secondary perpendicular external field (cross-flow) is applied. The cross-flow drives constituents toward the accumulation wall (a permeable membrane), but this force is opposed by the Brownian diffusion of the constituent particles. Larger particles (with low diffusivity) equilibrate at a relatively low mean elevation above the accumulation wall, where they migrate through the channel more slowly [46]. By contrast, smaller particles (with higher diffusivity) form a more diffuse layer that extends upward (i.e., has a higher mean elevation above the accumulation wall) and is thus able to sample faster streamlines nearer to the center of the parabolic flow profile; this increases their migration rate along the channel. Through the balancing of these forces, particles are separated into fractions according to their hydrodynamic size, with smaller particles eluting before larger ones. Equation 1 defines the retention ratio, R, and shows the inverse relationship between retention time (t_r) and particle diffusion coefficient (D) [44, 45].

$$R = \frac{t_0}{t_r}, \quad t_r = \frac{t_0 V_c w^2}{6DV_0} \tag{1}$$

Here, t_0 is the void time, V_0 is the channel void volume, V_c is the cross-flow rate, and w is the channel thickness (defined by the size of a rigid spacer).

In a manner analogous to SEC, various detectors can be incorporated in series to detect the elution of fractionated constituents and to characterize their properties. In the present case, we are primarily concerned with determining the in situ size of nanoscale constituents in aqueous media and differentiating between different components in multicomponent mixtures. This is relevant to the characterization of engineered

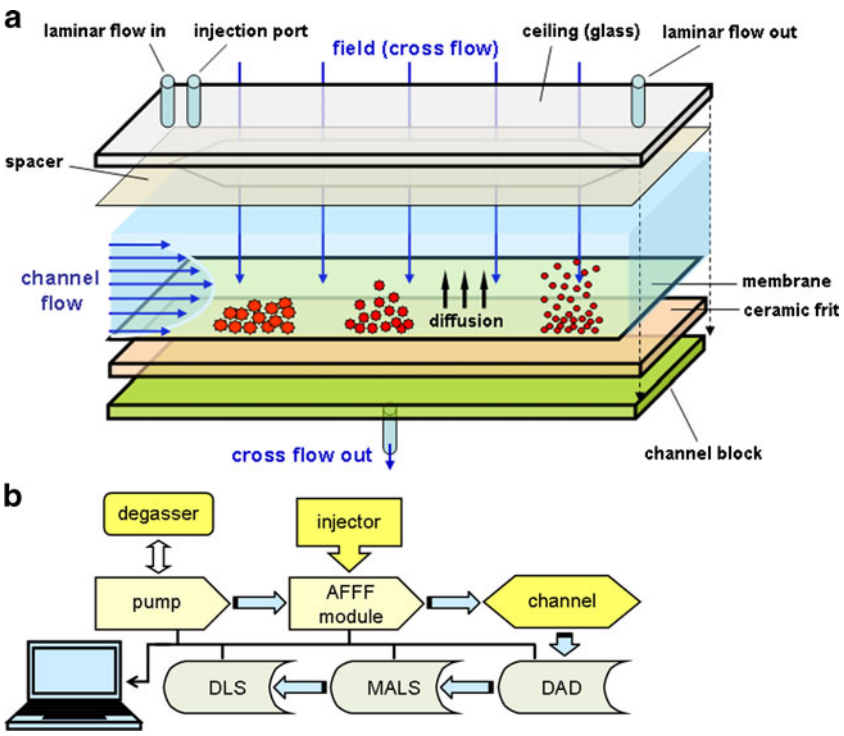

Fig. 1 **a** Schematic diagram of an AFFF fractionation channel illustrating the modes of flow and principle of hydrodynamic separation. **b** Flow chart showing flow and analysis chain as it was configured for the present study

nanoscale particles developed for biomedical or technical applications and to the analysis of environmental or industrial samples containing multiple unknown components. Size can be quantified by several methods, including multi-angle light scattering (MALS) to give the radius of gyration, dynamic light scattering (DLS) to give the hydrodynamic size, direct analysis of retention times (also provides a hydrodynamic size), and differential refractometry or viscometry to determine the molecular weight of macromolecular constituents. Fluorescence and absorption detectors can also be utilized to differentiate optically active components that differ in their composition or to identify specific labeled constituents. The elution process can be followed and tracked by continuously monitoring, for example, the scattering intensity at a fixed angle, the optical absorbance at one or more wavelengths, or the differential refractive index. Additional information can be obtained, depending on the specific instrument configuration and nature of the analyte, such as the relative proportion of monomers, dimers, and trimers in aggregation prone systems such as proteins.

Only a few reported studies have considered the characterization of GNPs using AFFF in any significant detail [47, 48], while sedimentation FFF (SdFFF) has been more widely applied perhaps due to the high bulk density of Au [49–51]. Song et al. [47] examined 5, 10, and 20 nm GNPs using AFFF and looked at the influence of the accumulation wall membrane in the presence of a nonionic surfactant in the mobile phase. They compared regenerated cellulose (RC) membrane with polysulfone and concluded that polysulfone caused a "disturbed" retention that they attributed to its wetting properties. More importantly, the authors showed that, for a given set of flow conditions, the surfactant formulation can significantly impact the retention time; these results bring into question the unambiguous determination of size from AFFF based solely on retention values, as retention can be impacted by other factors. Rameshwar et al. [48] looked at mercaptosuccinic acid (MSA)-capped GNPs and compared AFFF analysis with transmission electron microscopy (TEM) and off-line DLS. They found that AFFF yielded results that were much more consistent with the expected hydrodynamic size based on the known core size and an estimate of the MSA coating thickness, compared with either batch-mode DLS or TEM (using a staining procedure); however, their analysis and measurement optimization procedures were minimal, and they looked at a single GNP size (about 6 nm). More recently, Zattoni et al. [52] studied the retention and size analysis of polymer-coated GNPs using AFFF outfitted with a MALS detector. The radius of gyration was determined from the MALS data for the eluting GNPs, but again very little attention was given to method development. The most recently reported work is from Sermsri et al. [53], who focused on the effect of α-tocopherol in the citrate reduction of $HAuCl_4$ and used AFFF and TEM to characterize the reaction products. With the exception of Zattoni et al. [52], who used MALS, these previous studies did not address direct in situ measurement of size or the separation of individual GNP components within mixtures, both of which are addressed specifically in the present work. The present work also differentiates itself from previous efforts by a greater focus on optimization and method development for GNP analysis by AFFF.

We report the analysis of individual GNP components over a range of nominal sizes, specifically 10, 20, 30, 40, 50, and 60 nm, in an aqueous mobile phase and the fractionation of individual GNP components within multicomponent mixtures of the aforementioned materials. We examine the effects of various measurement and material parameters, including flow rates, membrane type, and mobile phase surfactants. Measurements were performed using a customized commercial AFFF system that incorporates in-line MALS, DLS, and UV–Vis absorbance detectors. The principal objectives of this work were to optimize measurement conditions for the analysis of GNPs and to develop measurement protocols that could then be applied for the characterization of GNPs under conditions that are relevant for biomedical research.

Experimental

Materials

Citrate-stabilized GNPs, nominally 10, 20, 30, 40, 50 and 60 nm, were obtained from Ted Pella, Inc. (Redding, CA)[1] and for brevity and clarity are referred to as GNP10, GNP30, etc.. The following chemicals were used without further purification: thiol terminated polyethyleneglycol (PEG-SH, molar mass (M=5 kDa) (NEKTAR, Huntsville, AL), sodium citrate ($Na_3C_6H_5O_7{\cdot}2H_2O$, ACS Reagent grade, Sigma-Aldrich, St. Louis, MO), sodium azide (NaN_3, 99%, Alfa Aesar, Ward Hill, MA), FL-70 detergent—according to the manufacturer, FL-70 contains 3.8% triethanolamine oleate, 2.7% sodium carbonate, 1.8% ethoxylated $C_{12–14}$-secondary alcohols, 1.4% tetrasodium ethylenediaminetetraacetate, 0.9% PEG, 0.5% sodium oleate, 0.1% sodium bicarbonate in water—(Fisher Scientific, Pittsburgh, PA), Triton X-100 nonionic surfactant ($[C_2H_4O]_x{\cdot}C_{14}H_{22}O$, MP Biomedicals, Solon, OH), sodium n-dodecyl sulfate anionic surfactant ($CH_3[CH_2]_{11}OSO_3Na$, 99%, Alpha Aesar), and cetyltrimethylammoniumbromide

[1] Certain trade names and company products are mentioned in the text or identified in illustrations in order to specify adequately the experimental procedure and equipment used. In no case does such identification imply recommendation or endorsement by National Institute of Standards and Technology; nor does it imply that the products are necessarily the best available for the purpose.

(CTAB) cationic surfactant (Molecular Biology Grade 98%, MP Biomedical, Solon, OH).

Preparation of PEG-ylated gold nanoparticles

Approximately 5 mL of native citrate-stabilized GNP suspension was placed into a clean glass vial followed by 500 μL of 2.5 mmol/L aqueous PEG-SH. The reaction mixture was stirred magnetically for 5 h at room temperature. After the reaction, the mixture was purified by filtration through a stirred ultrafiltration cell using a RC membrane (molecular weight cut off—MWCO=10 kDa). The filtrate (ca. 4 mL) was replaced with filtered deionized (DI) water; this procedure was repeated three times. The conjugation and purification procedures were carried out in a sterile clean bench. The mean z-average diameter of purified PEG-ylated gold particles was determined by replicate DLS measurements in batch mode. The results were as follows: 49.4±0.13 and 79.7± 0.5 nm, for nominally 30 nm Au-PEG (GNP30-PEG) and 60 nm Au-PEG (GNP60-PEG), respectively, where the uncertainty interval is the standard deviation of replicate measurements.

Instrumentation

The AFFF system used in this study (Fig. 1b) consists of a degasser (Gastorr TG-14, Flom Co., Ltd., Tokyo, Japan), high-performance liquid chromatography isocratic pump (1100 series, Agilent Technologies, Santa Clara, CA), manual injection valve (Rheodyne 7725i, IDEX Corporation, Oak Harbor, WA) with a 100 μL stainless steel sample loop, field/flow control module, and AFFF separation channel (Eclipse 2, Wyatt Technology, Santa Barbara, CA), MALS detector (Dawn Heleos, Wyatt Technology) with 15 scattering angles from 14.4° to 163.3°, and UV–Vis absorbance diode array detector (DAD1200, Agilent Technologies) with a spectral range from 190 nm to 950 nm and a sampling rate of 20 Hz. The instrument configuration uses a DLS device as the final detector (ZetaSizer-Nano, Malvern Instruments Inc., Westborough, MA) utilizing backscatter optics at a scattering angle of 173°. The AFFF separation channel (shown schematically in Fig. 1a) consists of a channel block, ceramic frit, permeable membrane (accumulation wall), spacer, and glass channel top.

Two membranes were utilized for AFFF experiments reported herein: RC (MWCO=10 kDa, Wyatt Technology) and polyvinylidene fluoride—PVDF—(MWCO 30 kDa, Sterlitech, Kent, WA). Hydrophilic RC is by far the most widely used membrane for AFFF studies involving aqueous phase analytes. PVDF was included to assess the impact of membrane chemistry on retention properties; PVDF presents a hydrophobic surface. Except where noted otherwise, study results correspond to use of RC membranes. A 350-μm spacer was used to define the depth of the AFFF channel for all separation experiments reported here. Other relevant channel dimensions were as follows: channel length 240 mm, channel breadth 21.5 mm (at inlet) and 6 mm (at outlet), and channel volume 1.8 mL.

Data acquisition for the MALS detectors was controlled by the ASTRA V software package. Data acquisition for the DAD1200 was controlled by Agilent ChemStation version B.02.01. Flow control in the Eclipse 2 system, including the AFFF channel, was provided through the Eclipse software version 2.0.04.

Measurement methods

The elution program (see Table 1 for specific conditions) was controlled through the software package provided with the Eclipse 2 instrument. For Programs A and B, the starting ratio of channel (laminar) flow to cross (field) flow was 0.5/1 and 1/2 mL/min, respectively. For both programs,

Table 1 Programmed AFFF experiment conditions used in this study. The channel-flow rate was held constant during each analysis

Program →	A	B	C	D
Injection+Focus	3 min	3 min	3 min	3 min
Focus	5 min	5 min	5 min	5 min
Elution-1	20 min	20 min	20 min	20 min
	ChF 0.5 CF 0.5→0 (A0.5)	ChF 1.0	ChF 0.5	ChF 1.0
	CF 1.0→0 (A) CF 1.5→0 (A1.5)	CF 2.0→0	CF 1.0	CF 2.0
Elution-2	40 min	40 min	20 min	20 min
	ChF 0.5	ChF 1.0	ChF 0.5	ChF 1.0
	CF 0	CF 0	CF 1.0→0	CF 2.0→0
			20 min	20 min
			ChF 0.5	ChF 1.0
			CF 0	CF 0

ChF channel-flow, *CF* cross-flow; both in milliliter per minute

the cross-flow was linearly reduced from its initial value to 0 over a period of 20 min. Following the field decay, channel-flow continued for an additional 40 min. In Programs C and D, the initial cross-flow of 1 and 2 mL/min, respectively, was kept constant for the first 20 min, then allowed to decay linearly to 0 over the subsequent 20 min. The channel-flow for Programs C and D was 0.5 and 1 mL/min, respectively; channel-flow was continued for an additional 20 min following field decay. The elution programs were developed to investigate the effect of applied field and flow rates on the retention behavior of GNPs and the quality of data obtained during elution (e.g., peak resolution and noise).

All GNP samples were prepared for analysis by dilution of native solution into DI water (on a volume basis) in the following proportions: 1:2 for GNP10 and 1:10 for GNP20-GNP60. For multicomponent GNP samples, M3 (GNP10+ GNP20 + GNP30) and M5 (GNP10 + GNP20 + GNP30 + GMP40 + GNP60), the diluted solutions were then combined (on a volume basis) in the following ratios: 2:1:1 for M3 and 2:1:1:1:0.5 for M5. The native GNP suspensions were nominally identical in terms of the Au mass fraction. DI water (18 MΩ-cm resistance) was refiltered prior to use using a polyethersulfone membrane with 0.1 μm pore size. Prepared GNP samples were filtered prior to analysis using a 0.45-μm pore size PVDF syringe filter. An injection volume of 100 μL was used for all experiments; an excess volume was introduced to the injector to ensure repeatability of the injected volume. Blank tests (injection of mobile phase with no GNPs) were performed under the appropriate conditions just prior to GNP experiments.

The chromatographic trace (fractogram) was registered by continuously monitoring one of the DAD channels fixed at a wavelength of 520 nm (i.e., near the characteristic surface plasmon resonance—SPR—absorption band for GNPs in this size range) and the MALS signals. For MALS, only data from the detector positioned at a scattering angle of 90° is reported here and is referred to simply as the light scattering (LS) trace. Full UV–Vis absorbance spectra were obtained using the in-line DAD detector, to provide assurance that eluting peaks were in fact GNPs and not artifacts or contaminating particles

The z-average effective spherical hydrodynamic diameter, D_z, was determined by DLS based on the cumulants analysis [54] of the scattered intensity autocorrelation functions measured across each eluting peak. Figure 2 shows an example trace for GNP30. The D_z values recorded within the specified retention time range (e.g., see vertical bars in Fig. 2) were averaged to generate a mean D_z for each eluting peak. This range was defined by the trace peak width and by the noise level and constancy of the size data. The mean value is reported along with the uncertainty (one standard deviation about the mean), where uncertainty reflects the observed precision for a series of independent measurements across the peak and does not explicitly include other possible contributions such as fitting error, correlation baseline noise, or multiple scattering (unlikely under the conditions of this study). Similarly, the uncertainty reported for retention time (t_r) is one standard deviation of replicate AFFF measurements (three to five replicates).

All measurements were conducted at 20±0.1 °C, but temperature was directly controlled only in the MALS and DLS cells. Eluting samples were subject to ambient temperatures outside of these cells, where the ambient temperature was generally within 2 °C of the experimental temperature.

Results and discussion

In order to evaluate the potential of AFFF method development in a DI water mobile phase, we investigated the retention

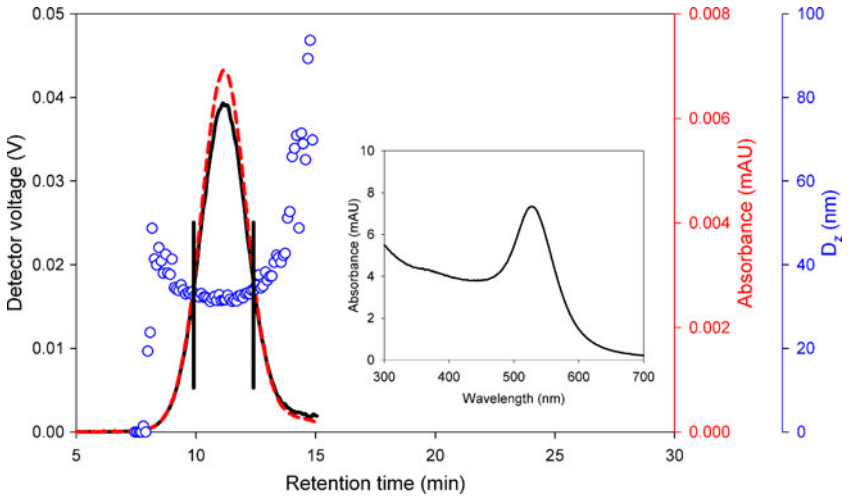

Fig. 2 Representative fractogram for GNP30 showing UV absorption trace at 520 nm (*dashed line*), MALS trace at 90º (*solid line*) and z-average hydrodynamic diameter, D_z (*open circles*). *Inset* shows full-range UV–Vis spectrum obtained on-line for eluting peak

behavior of individual Au NPs in DI water without additives. Figure 3 shows fractograms measured for GNP30 and GNP60 eluted in a DI water mobile phase as a function of cross-flow rate and at a fixed channel-flow rate of 0.5 mL/min (Program A). Real time UV–Vis spectra (not shown) confirmed that all peaks can be attributed to GNPs (i.e., characteristic SPR absorption was observed), including the void peak (designated as t_0). To explore the range of behavior associated with variation of the cross-/channel-flow ratio, the cross-flow rate was set to 0.5, 1, and 1.5 mL/min (corresponding to Programs A0.5, A, and A1.5, respectively, in Table 1).

Although theoretically the size of eluting particles can be estimated based on the retention time and known channel and flow parameters, from a practical standpoint it is far easier and more direct to measure size using MALS or DLS in flow-mode operation. For the particle size range under consideration here, the mean D_z determined from DLS is utilized. DLS yields size results for GNPs that are consistent across experiments and correspond closely with off-line batch measurements of the same test particles.

The measured peak retention time and corresponding D_z values for GNP30 eluted in DI water were as follows: t_r= 3.1 min, D_z=30.3±0.9 nm for Program A0.5; 3.5 min, 30.3± 1.1 nm for Program A and 30.8±0.9 nm for Program A1.5. For GNP60, the results were: 4.8 min, 60.1±1.2 nm for Program A0.5; 5.7 min, 60.3±1.2 nm for Program A and 60.0±1.5 nm for Program A1.5.

Results show that at 0.5 mL/min the cross-flow rate is insufficient to fully retain the GNPs, resulting in "unretained" GNPs eluting within the void peak. The void peak itself, which elutes consistently at t_r≈1.2 min, decreases in intensity with increasing cross-flow rate (1.0 mL/min) as the GNP retention improves. While the void peak retention time is insensitive to cross-flow rate, retention of "retained" GNPs in Fig. 3 increases as the cross-flow rate is increased from 0.5 to 1.0 mL/min; however, above a cross-flow rate of 1.0, the retention time appears to stabilize. The lack of increased retention at higher cross-flow appears to contradict the relationship established in Eq. 1; however, the very low ionic strength associated with the DI water mobile phase induces an enhanced repulsive force [47] between the GNPs and the hydrophilic membrane surface. This additional repulsion appears to place a maximum on the retention time achievable in this case, though this explanation is admittedly somewhat speculative.

At a cross-flow rate of 1.5 mL/min, the void peak is barely discernable, but the appearance of a third peak or shoulder at t_r≈5.5 min in the GNP30 fractogram suggests either the formation of aggregates or the presence of "over-retained" GNPs, perhaps due to excessive downward force on the particles flowing near the accumulation wall. This feature does not appear for GNP30 under other elution conditions, further suggesting it is an artifact of the elution process rather than a native component within the GNP30 itself. Unfortunately, this peak area is too small to measure the size reliably, thus the identity of this peak is not entirely clear; it is also interesting to note that this effect is not observed for the larger GNP60.

Effect of citrate and mobile phase ionic strength

Because the GNPs are citrate capped, sodium citrate solutions were investigated for use as a chemically compatible mobile phase. The use of citrate salts also enabled us to examine the effect of ionic strength (I) on retention behavior. To begin with, we evaluated the effect of flow rate ratio on retention behavior for GNP30 in a 0.005% (I=1.0 mmol/L) citrate mobile phase using the

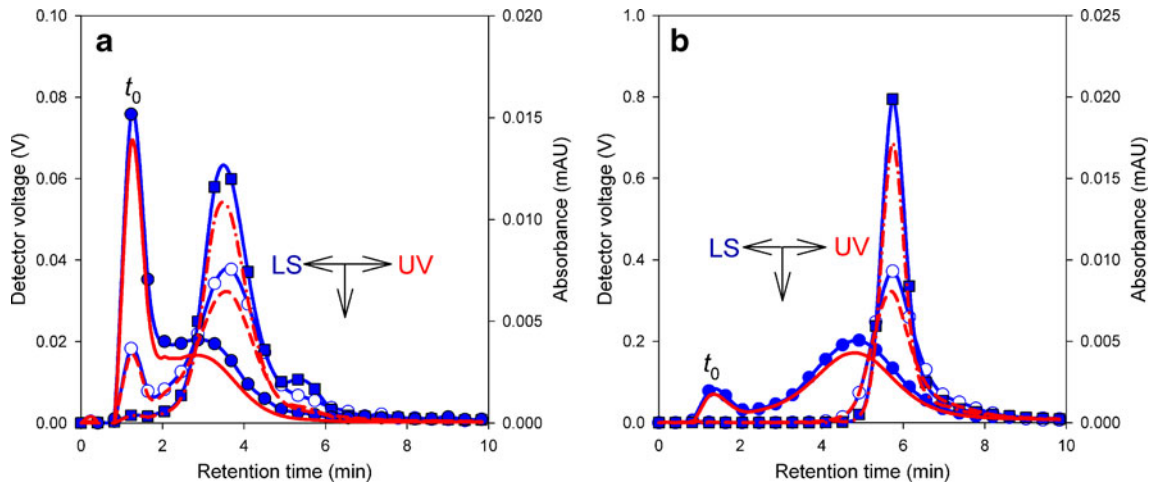

Fig. 3 AFFF fractograms with DI water as mobile phase for **a** GNP30 and **b** GNP60: 90° MALS (LS)/UV traces: (*closed circles*)/(*solid line*) Program A0.5; (*open circles*)/(*dashed line*) Program A; (*closed squares*)/(*dash-dotted line*) Program A1.5

Program A series. In comparison to the DI water mobile phase, in citrate t_r is 6.7 min [D_z=30.3±1.0 nm], 8.9 min [31.0±1.0 nm], and 10.5 min [30.9±0.9 nm], for Programs A0.5, A, and A1.5, respectively (fractograms not shown). Clearly, retention times are retarded in the presence of citrate, relative to DI water, and much more differentiated with respect to the flow rate ratio. The results indicate greater interaction between the GNPs and the membrane surface when citrate is present in the mobile phase, perhaps as a result of charge screening provided by the triply charged citrate and Na^+ ions (RC has a residual negative charge [48], as do the GNPs); essentially, the particles can approach closer to the membrane surface (accumulation wall) of the AFFF channel, thus increasing retention while improving separation [47, 55, 56].

To study the effect of varying the mobile phase ionic strength, solutions containing citrate mass fractions of 0.005%, 0.01%, 0.05%, and 0.1% (corresponding to I (mmol/L)=1.0, 2.0, 10.2 and 20.4, respectively) were used in conjunction with Program A (channel/cross-flow=0.5/1). The results are summarized in Fig. 4a–d.

As shown in Fig. 4c, t_r increases more than threefold with increasing ionic strength, then approaches a plateau level above 20 mmol/L. At the same time, particle size associated with the eluting GNP peak (Fig. 4d, Table 2) is stable up to about 10 mmol/L, above which the mean D_z begins shifting upward indicating that the screening effect of the salt is beginning to degrade the stability of the GNPs resulting in some dimer formation. The coincidence of the UV peak measured at 520 nm and the LS peak (fractograms in Fig. 4a, b) verifies that these "events" are associated with the GNPs.

The UV trace, which primarily tracks GNP concentration, exhibits some variation versus ionic strength in the case of

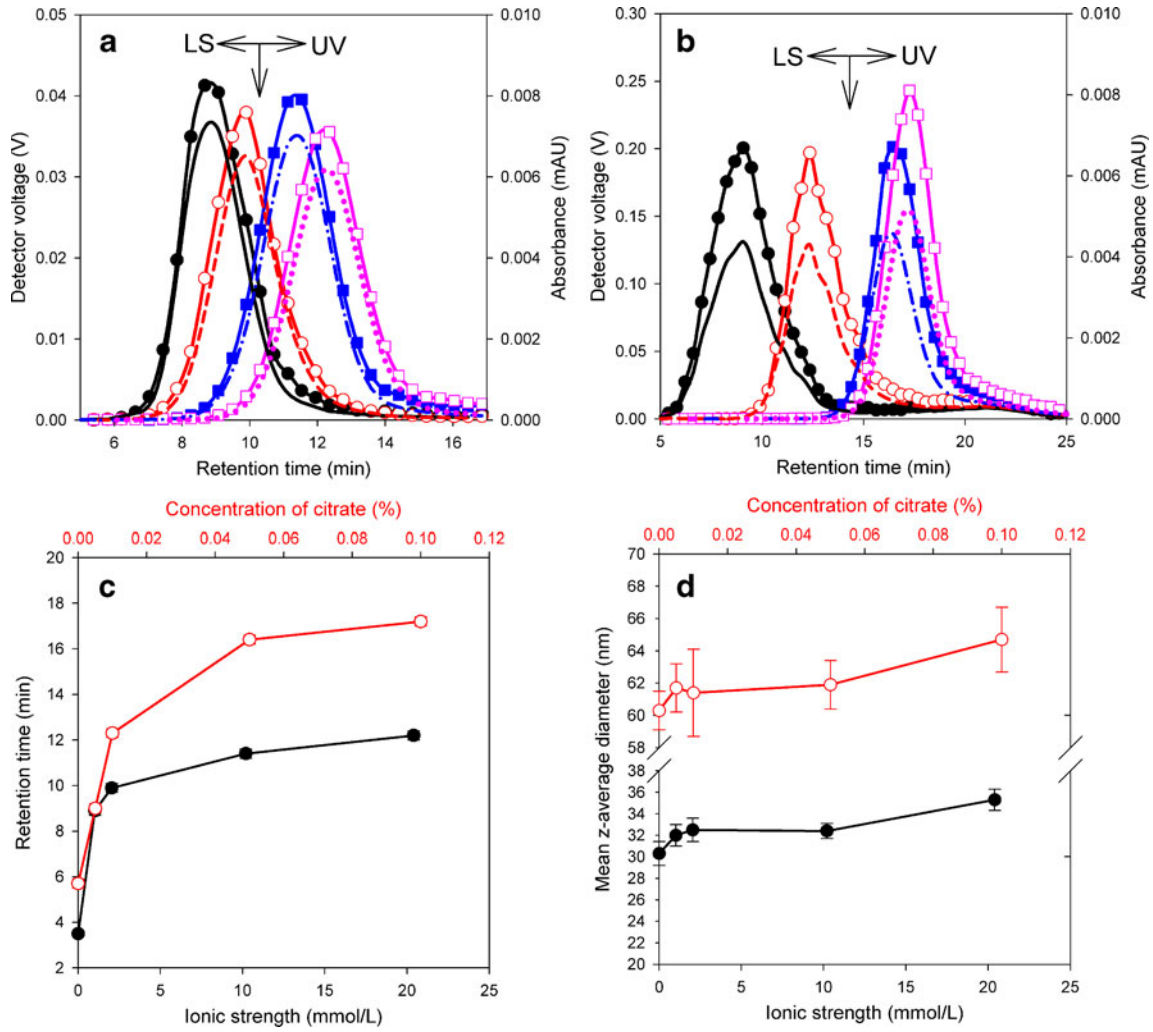

Fig. 4 AFFF fractograms (Program A) for **a** GNP30 and **b** GNP60 as a function of sodium citrate concentration: 90° MALS (LS)/UV traces: (*closed circles*)/(*solid line*) 0.005%; (*open circles*)/(*dashed line*) 0.01%; (*closed squares*)/(*dash-dotted line*) 0.05%; (*open squares*)/(*dotted line*) 0.1% sodium citrate. Variation of retention time **c** and mean z-average diameter **d** of GNPs (*closed circles* 30 nm, *open circles* 60 nm) with various ionic strength

Table 2 Summary of AFFF characterization results for GNP30 and GNP60 as a function of the mobile phase composition

Mobile phase (I, mmol/L)	Retention time (min)[a]			Mean z-average diameter (nm)[b]	
	GNP30 (R)[c]	GNP60 (R)[c]	$\Delta\ t_{r<60\text{-}30>}$	GNP30	GNP60
DI water	3.5±0.1 (0.34)	5.7±0.2 (0.21)	2.2	30.3±1.1	60.3±1.2
0.005% CT (1.0)	8.9±0.2 (0.10)	9.0±0.2 (0.10)	0.1	32.0±1.0	61.7±1.5
0.01% CT (2.0)	9.9±0.2 (0.09)	12.3±0.2 (0.073)	2.4	32.5±1.1	61.4±2.7
0.05% CT (10.2)	11.4±0.2 (0.079)	16.4±0.2 (0.055)	5.0	32.4±0.7	61.9±1.5
0.1% CT (20.4)	12.2±0.2 (0.074)	17.2±0.2 (0.052)	5.0	35.3±1.0	64.7±2.0
0.02% AZ (3.1)	11.1±0.2 (0.081)	16.0±0.2 (0.056)	4.9	32.8±0.7	59.0±2.2
0.05% SDS (1.7)	9.8±0.2 (0.092)	14.8±0.2 (0.061)	5.0	32.1±1.2	60.1±2.2
0.05% SDS in 0.02% AZ (4.8)	10.3±0.2 (0.087)	15.4±0.2 (0.058)	5.1	34.2±1.2	60.4±2.5
0.1% SDS in 0.02% AZ (6.6)	10.2±0.2 (0.088)	15.6±0.2 (0.058)	5.4	35.6±2.0	62.6±3.0
0.05% FL-70	9.5±0.2 (0.095)	13.9±0.2 (0.065)	4.4	40.2±1.2	66.6±2.0

CT sodium citrate, *AZ* sodium azide

[a] All measurements were conducted using identical flow rate conditions (see Program A), pump pressure 9.6–9.8 bar (0.96–0.98 MPa), continuous runs on same membrane sheet

[b] Flow-mode DLS measurement

[c] Retention rate from Eq. 1; void retention times (t_0) in various mobile phases were determined from void peak center in each measured fractogram; all t_0 appeared at 0.9±0.05 min except in DI water (≈ 1.2 min)

GNP30 (Fig. 4a, lines with no symbols), with perhaps a slight downward trend indicating some irreversible loss of GNP to the membrane with increasing citrate concentration. For GNP60 (Fig. 4b), the UV trace indicates a stable GNP recovery, unaffected by citrate concentration. The R values (Eq. 1) for both GNP30 and GNP60 for the series of citrate mobile phase solutions are in the range from 0.025 to 0.1 ($t_0 \cong$ 0.9, Table 2), which is within the generally recommended range for AFFF [44]. The differential retention time for GNP30 versus GNP60 in citrate mobile phase (mass fraction trisodium citrate, $\Delta t_{r60\text{-}30}$: 0.005%, 0.1 min; 0.01%, 2.4 min; 0.05%, 5.0 min; 0.1%, 5.0 min) can be used as a metric for the resolving power associated with a particular experimental set up. Clearly, the resolution is enhanced by the addition of citrate up to about 0.05%, beyond which the two peaks cannot be further separated and the increase in citrate becomes detrimental to GNP stability (as reflected by the uptick in GNP size at 0.1% citrate).

Effect of surfactants in mobile phase

Surfactants are frequently utilized in AFFF separations, where they may improve retention properties, prevent particle aggregation during analysis, and reduce loss of analyte to the accumulation membrane [44]. We examined a series of common surfactant formulations to determine their impact on GNP characterization and separation. Additives examined include anionic sodium dodecyl sulfate (SDS), a detergent containing both anionic and nonionic surfactants (FL-70), nonionic Triton X-100, and cationic cetyltrimethylammoniumbromide. Additionally, we looked at the impact of sodium azide (NaN_3), a biocide commonly included in carrier solutions to prevent bacterial growth. The fractograms (with Program A) and size data for GNP30 and GNP60 with various carrier solutions are shown in Figs. 5 and 6 and summarized in Table 2. As expected, the elution of GNPs in aqueous NaN_3 (mass fraction 0.02%, I=3.1 mmol/L) occurred slightly earlier (t_r=11.1 and 16.0 min for GNP30 and 60 nm GNPs, respectively) relative to our designated "control" (0.05% citrate) mobile phase (11.4 and 16.4 min for GNP30 and GNP60, respectively), an effect that can be attributed to the difference in ionic strength between the two solutions.

By contrast, the surfactant formulations exhibited more complex behavior. For instance, in 0.05% SDS with 0.02% NaN_3 added (I=4.8 mmol/L), GNPs eluted significantly earlier (10.3 min for GNP30, 15.4 min for GNP60) than in the control (I=10.2 mmol/L), which correlates with the ionic strength effect on retention behavior. However, GNPs in the SDS/NaN_3 mobile phase also eluted faster compared with GNPs in 0.02% NaN_3 alone (I=3.1 mmol/L), despite the relatively higher ionic strength in the SDS/NaN_3 solution. This suggests that SDS also acts to reduce the interaction between the GNPs and the membrane surface, an effect that is convoluted with the electrostatic screening effect.

In 0.05% FL-70, a widely used formulated detergent, the retention time was further reduced relative to SDS (9.5 and 13.6 min, for GNP30 and GNP60, respectively) with a significant increase in mean D_z (40.2±1.2 and 66.6± 2.0 nm, respectively). FL-70 produced the fastest GNP elution and the largest GNP mean size among any carrier

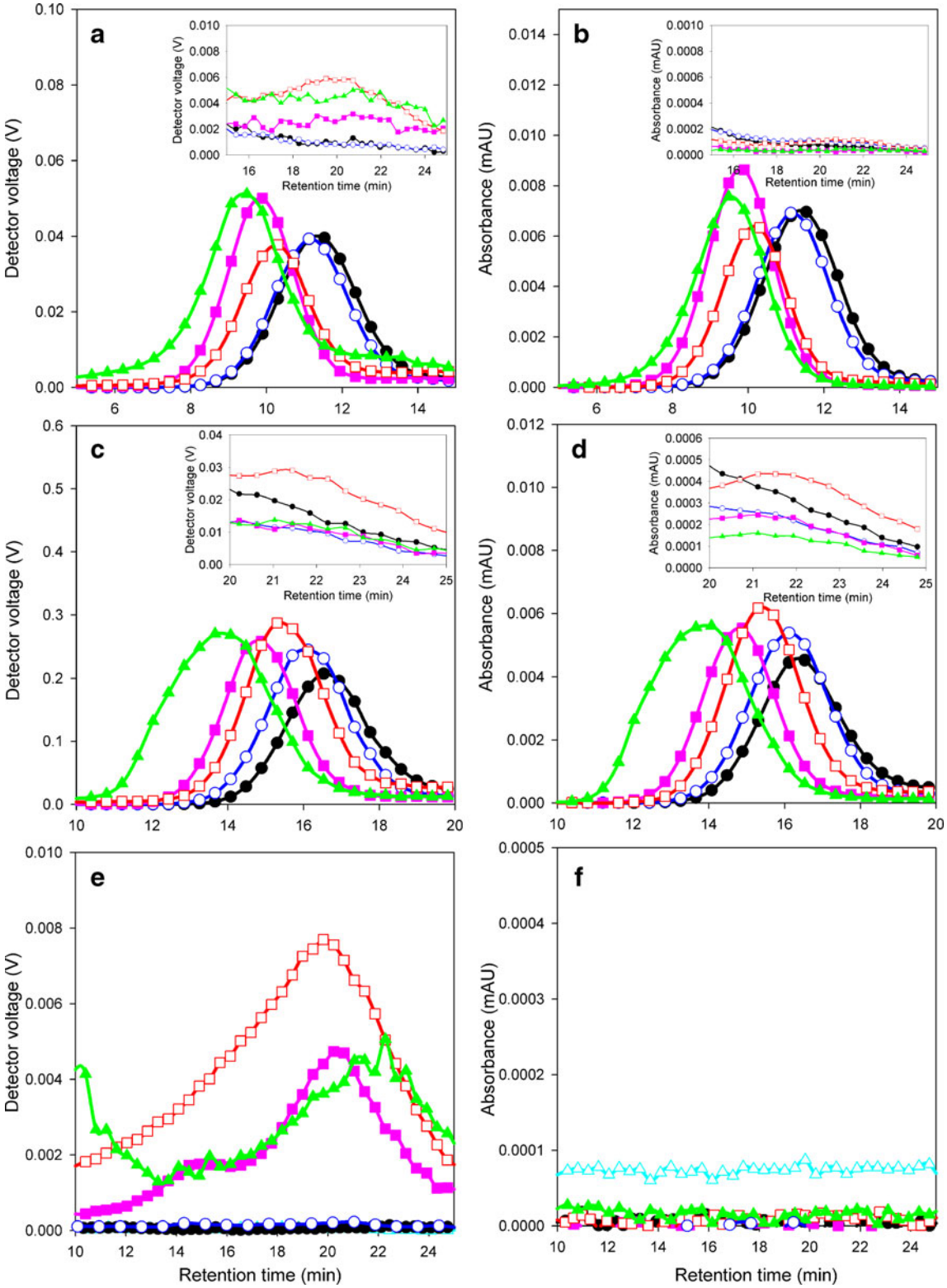

Fig. 5 Fractograms (Program A) for GNP30 (**a** 90° MALS (LS) trace, **b** UV trace), GNP60 (**c** LS trace, **d** UV trace) and blank tests (**e** LS trace, **f** UV trace) with various mobile phases. LS/UV traces: (*closed circles*) 0.05% sodium citrate; (*open circles*) 0.02% NaN_3; (*open squares*) 0.05% SDS in 0.02% NaN_3; (*closed squares*) 0.05% SDS; (*closed triangles*) 0.05% FL-70; (*open triangles*) DI water (only in blank tests)

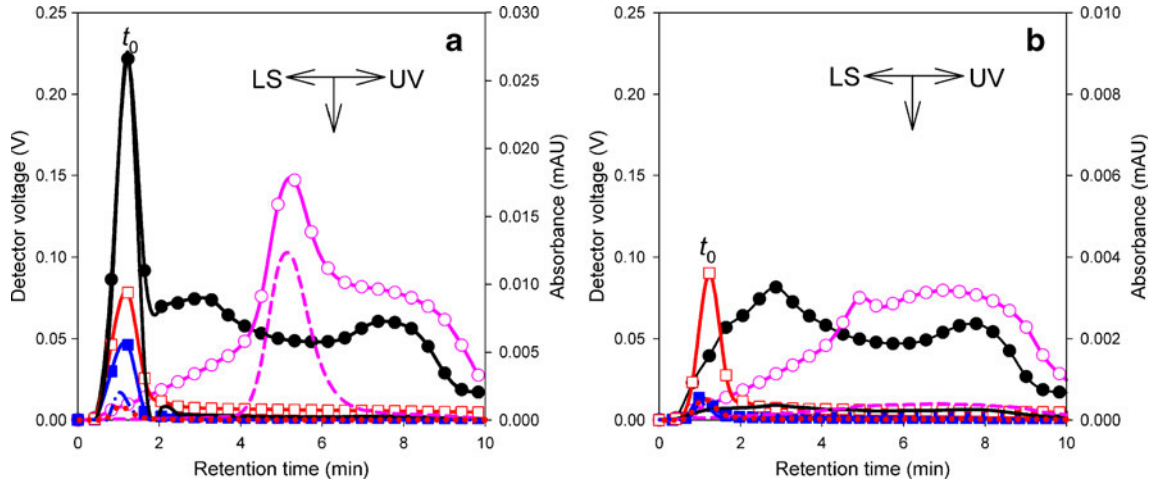

Fig. 6 AFFF fractograms for **a** GNP30 and **b** control tests with Triton X-100 and CTAB mobile phase without GNPs. 90° MALS (LS)/UV traces: (*closed circles*)/(*solid line*) 0.05% Triton X-100; (*open circles*)/(*dashed line*) 0.05% Triton X-100 in 0.02% NaN_3; (*closed squares*)/(*dash-dotted line*) 0.05% CTAB; (*open squares*)/(*dotted line*) 0.05% CTAB in 0.02% NaN_3

solution evaluated in this study (see Table 2). Thus, the surfactant activity of FL-70 is relatively strong, greatly reducing the interaction between the GNPs and the membrane surface. But at the same time, FL-70 induces a substantial increase in size, either as a result of cluster formation or due to the adsorption of surfactants from the mobile phase. The difference in the SPR peak position between citrate and FL-70 mobile phases is only about 2 nm, so it is not possible to definitively attribute the observed D_z increase either to clusters or surfactant adsorption; in fact, it could be a combination of the two effects. The complex nature of FL-70 makes it nearly impossible to assess potential interactions, as it contains nonionic species (PEG, ethoxylated $C_{12–14}$ secondary alcohol), anionic species (sodium oleate), and even amine-containing species (triethanolamine oleate, tetrasodium ethylenediaminetetraacetate), all of which are potentially surface active toward GNPs.

The surfactant effect can also be counterproductive with respect to resolving power; by accelerating the elution of GNPs, their separation (fractionation) is thereby reduced. Of the mobile phase compositions used in the present study, viz. (1) 0.05% sodium citrate, (2) 0.02% NaN_3, (3) 0.05% SDS, (4) 0.05% SDS with 0.02% NaN_3, and (5) 0.05% FL-70, solution 2 exhibited the best signal profile with respect to balancing retention and resolution. In the case of solutions 3, 4, and 5, a very weak and broad LS peak or shoulder was observed between about 13 and 25 min during the elution of GNP30 using Program A (see Fig. 5). There are several possible explanations for this spurious peak: particle aggregation during elution, slow release of excessively retained particles, carryover (contamination) from previous measurements, impurities from the surfactant solution, or micelle formation. The results of blank tests performed on each mobile phase (without GNPs) are presented in Fig. 5e (LS trace) and Fig. 5f (UV trace) and clearly show the appearance of the spurious peaks to be associated with the mobile phase. Since the peaks only appear in the presence of surfactants and are not evident in the 520 nm UV trace, impurities and/or micelle formation seem to be the most likely origin. Furthermore, as the peak occurs for two different surfactant formulations, impurities can probably be ruled out as well. We are left to conclude that these peaks arise from the formation of micelles, even though the concentration of surfactant in mobile phases 3, 4, and 5 is far below the critical micelle concentration (CMC) value for SDS (0.236% or 0.0082 mol/L) [57] and for FL-70 (5.1%) [53]. Presumably, the focusing and cross-flow may lead to the formation of micelles even at fairly low surfactant concentrations. This phenomenon deserves further attention in the future.

Complicating this picture further, in the case of GNP60, extended tails and/or weak shoulders are apparent even in mobile phases 1 and 2, in both the MALS and the UV traces (Fig. 5c, d). UV absorption at 520 nm indicates that these tails/shoulders contain GNPs and are not entirely attributable to the mobile phase artifact. In AFFF, particles are driven by the field toward the accumulation wall, and this downward force is balanced by diffusion-driven transport away from the wall. As a result of these counter-acting forces, the larger GNP60 find their equilibrium location closer to the membrane surface compared with the smaller GNP30. Therefore, GNP60 has a greater opportunity to be absorbed or excessively retained on the membrane, and this could cause retarded elution of trace quantities of particles resulting in peaks that are elongated in time. It is also possible that the tails are due to small GNP aggregates formed during the focusing step, but this cannot be confirmed by DLS due to the low signal intensity.

Fractograms for GNPs measured in 0.05% Triton X-100 (octylphenol polyethoxylate) nonionic surfactant mobile phase exhibited unusually large void peaks in both the MALS and UV traces (see, e.g., Fig. 6a) and generated additional broad and distorted peaks in the MALS trace (some of which have no corresponding UV-520 signal). This suggests that the eluting GNPs are mostly contained within the void peak and that, like SDS and FL-70, Triton X-100 (CMC=0.015%) [57] produces micelles and possibly micelle aggregates within the eluting mobile phase. By comparing UV520 peak areas for Triton X-100 and citrate (Fig. 5b), we estimate 80% of the GNP30 load is eluted within the void peak for Triton X-100. Interestingly, when measured in a mobile phase containing both Triton X-100 and NaN_3, the void peak vanishes, and a very broad MALS peak appears with a narrow GNP peak (identified by the UV trace at 520 nm) buried within (see Fig. 6a). The broad peaks that appear in the MALS trace for Triton X-100 and Triton X-100/NaN_3 are reproduced in control experiments containing no GNPs (Fig. 6b). So, the large void peak associated with Triton X-100 in the mobile phase only occurs in the presence of GNPs and must be attributed to interactions between the surfactant and the particles.

Finally, in a mobile phase containing 0.05% CTAB (CMC=0.035%) [57], a cationic surfactant with and without 0.02% NaN_3, the apparent GNP recovery drops precipitously, and a relatively large (i.e., compared with citrate or NaN_3 alone) void peak appears in both MALS and UV traces. Clearly, CTAB is an inappropriate choice for AFFF analysis of the GNPs used in the present study. CTAB, being a cationic surfactant, probably destabilizes the negatively charged GNPs, causing them to "crash out" and adhere to the membrane. Some of this material manages to be entrapped in the void peak, as indicated by the small peak in the UV trace. A blank fractogram for CTAB without GNPs present (Fig. 6b) exhibits a large void peak in the MALS trace, while in the absence of NaN_3 the void peak collapses. Neither mobile phase exhibits the broad features associated with the anionic and nonionic surfactants, suggesting that CTAB is immune from micelle formation under the conditions of the AFFF experiment or that any associative structures that are formed must be such weak scatterers that they are essentially below the detection limit for this system.

Analysis of multicomponent GNP mixtures

At the next level of analysis, we focus specifically on mobile phases 1, 2, and 4 and examine their ability to fractionate and characterize *multicomponent* GNP mixtures using AFFF. The retention and size results for individual GNPs with nominal sizes ranging from 10 to 60 nm, and using these three different mobile phases, are summarized in Table 3 and will serve as a baseline comparison for results obtained on multicomponent mixtures of these GNPs.

The first multicomponent test sample, referred to here as M3, is a mixture of GNP10, GNP30, and GNP60, formulated as described in the "Experimental" section. M3 was fractionated according to Program A in a mobile phase of 0.02% NaN_3 (solution 2). The results of this experiment are shown in Fig. 7, where the fractograms are overlaid with those from individually measured GNPs for comparison. The three components were easily separated, with nearly baseline resolution. The measured retention times were identical to the corresponding individual

Table 3 Summary of AFFF characterization results for GNPs with mobile phase containing sodium citrate, sodium azide or sodium azide with SDS

GNPs→Size (nm)[a]	GNP10 (11.5±0.1)	GNP20 (21.2±0.1)	GNP30 (28.0±0.2)	GNP40 (39.6±0.2)	GNP50 (47.2±0.2)	GNP60 (55.4±0.3)
Mobile phase ↓	Retention time[b] (min)					
	Mean z-average diameter[c] (nm)					
0.05% CT	5.3±0.1	9.0±0.1	11.4±0.2	13.8±0.2	15.5±0.2	16.4±0.2
	12.6±0.8	26.4±1.5	32.4±0.7	42.0±0.5	50.0±0.7	61.9±1.5
0.02% AZ	5.4±0.1	9.0±0.1	11.1±0.2	13.5±0.2	14.7±0.2	16.0±0.2
	14.3±0.5	24.4±0.6	32.8±0.7	43.8±0.7	50.4±1.2	59.0±2.2
0.05% SDS in 0.02% AZ	5.0±0.1	8.7±0.1	10.3±0.2	12.8±0.2	14.0±0.2	15.4±0.2
	14.8±0.6	25.0±1.2	34.2±1.2	43.2±1.2	50.4±1.7	60.4±2.5

CT sodium citrate, *AZ* sodium azide

[a] z-average from batch-mode DLS measurement of neat samples

[b] Measured by Program A; pump pressure is 9.6–9.8 bar (0.96–0.98 MPa); continuous runs on same membrane sheet. Retention time varied slightly with pump pressure and on different membrane sheets

[c] Flow-mode DLS measurement

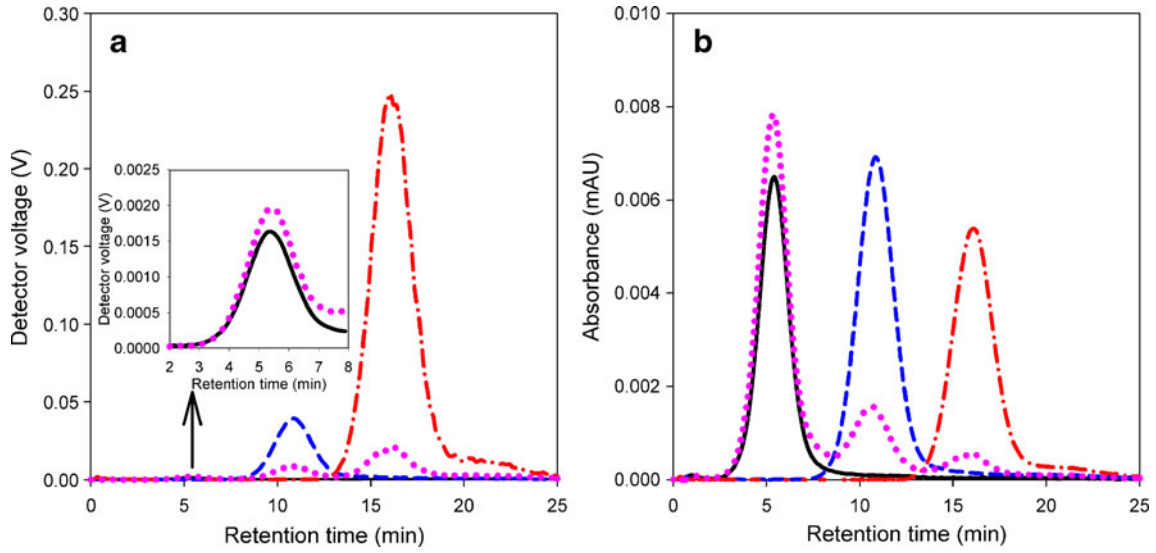

Fig. 7 AFFF fractograms (Program A) for each individual GNP and their mixture (M3) in 0.02% NaN_3 mobile phase. **a** 90° MALS (LS) trace; **b** UV trace: (*solid line*) GNP10, (*dashed line*) GNP30, (*dash-dotted line*) GNP60, (*dotted line*) M3 mixture

measurements performed under the same conditions. The strong UV signals in the multicomponent mixture (Fig. 7b) confirm the assignment of these peaks to GNPs with their characteristic SPR band near 520 nm.

Building on this success, we next examine a mixture containing five components spaced more closely, viz., 10, 20, 30, 40, and 60 nm GNPs, a mixture that we refer to here as M5. As shown in Fig. 8a, the resolving power of Program A was not sufficient to adequately separate the components in M5, though they can be identified by their corresponding maxima. Next, by varying the channel-flow and/or cross-flow rates, we set up different running conditions referred to as Programs B, C, and D in Table 1.

Fractograms for M5 obtained using Program B (Fig. 8b) show marked improvement in peak separation compared with Program A, though the peaks still overlap; this is particularly evident in the UV trace. The improvement is induced by doubling both the channel and cross-flow rates relative to Program A. In Program C, the channel/cross-flow ratio is identical to Program A (0.5:1.0 mL/min), but the cross-flow field is held constant during the initial 20 min then allowed to decay to zero linearly during the next 20 min. So, essentially, the magnitude of the applied field and laminar flow are the same in Programs A and C, but in the latter the particles are subjected to the maximum cross-flow field for a longer period of time. This allows the components to better separate into fractions, with delayed retention times. The result, shown in Fig. 8c, is an incremental improvement over Program B; however, the GNP20 and GNP30 peaks remain convoluted.

In Program D, we double both the channel- and cross-flow rates used in Program C (1.0:2.0 mL/min), with the maximum cross-flow field being applied for the same 20 min time period before allowing it to decay. The Program D fractogram, shown in Fig. 8d, yields well-separated GNP fractions with minimal convolution, but with a significant reduction in GNP recovery (as indicated by the reduced MALS and UV signals). The corresponding mean D_z values for the M5 fractions (Program D) were as follows, proceeding left to right in Fig. 8d: 12.7±1.1, 26.4±1.6, 34.1±1.3, 42.3±1.9, and 59.7±2.1 nm. UV–Vis absorption spectra were recorded with the on-line DAD for each eluting fraction and are shown in Fig. 8e. The absorption spectra correlate with the size data, exhibiting a red shift in λ_{max} corresponding with the increase in GNP core size. The λ_{max} values were observed at 522, 524, 528, 532, and 536 nm, respectively, for 10, 20, 30, 40, and 60 nm GNP fractions. By comparison, the batch-mode (i.e., unfractionated) DLS analysis of M5 (see intensity-weighted distribution in Fig. 8f) does not provide useful or representative size information. It is simply not possible to deconvolute such closely spaced peaks using DLS alone; The "one pot" DLS measurement yields a broad amalgam representing the component populations and strongly weighted toward the larger size population as predicted for Rayleigh scatterers [58].

Retention and fractionation of PEG-ylated GNPs

In addition to negatively charged citrate-stabilized GNPs discussed thus far, we have also examined the application of our methodology to neutral PEG-conjugated GNPs created from the same core citrate GNPs, as well as mixtures of PEG-ylated and unconjugated GNPs. PEG-conjugated GNP30 (GNP30-PEG; 49.4±0.13 nm by batch DLS) and GNP60 (GNP60-PEG; 79.7±0.5 nm by batch

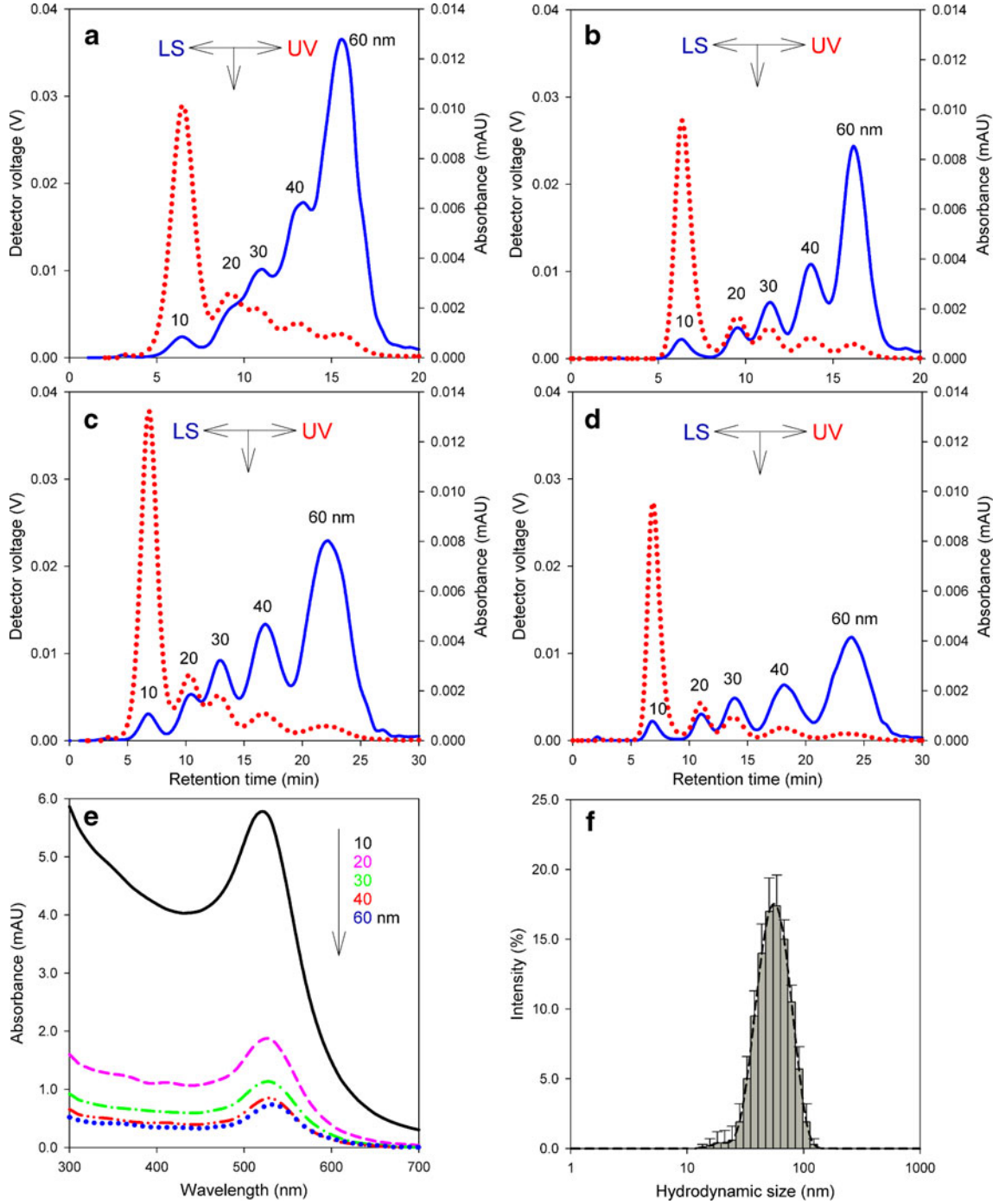

Fig. 8 AFFF fractograms of M5 GNP mixture in 0.02% NaN_3 mobile phase. 90° MALS (LS)/UV traces (*solid line*)/(*dotted line*) for (**a**–**d**). **a** Program A; **b** Program B; **c** Program C; **d** Program D; **e** UV–vis spectra of separated GNP fractions obtained for eluting peak through DAD; **f** batch-mode DLS size distribution for mixture M5 obtained using a vendor-supplied non-negative least squares inversion algorithm

DLS) were analyzed using Programs C and D, respectively. Additionally, mixtures of the PEG-ylated and native core particles were fractionated using the same programs. Representative fractograms are shown in Fig. 9.

The PEG-ylated GNPs exhibited delayed retentions relative to their citrate-stabilized analogs, as a result of the increase in hydrodynamic size afforded by the surface adsorbed PEG molecules. Furthermore, the fractograms for the conjugated GNPs exhibited a single well-defined peak with no evidence of unconjugated or aggregated GNPs, which confirms that the conjugation procedure was successful in forming stable monodisperse coated particles. Flow-mode DLS measurements on the eluting peaks corresponding to the 30-PEG and 60-PEG GNPs yielded hydrodynamic sizes of

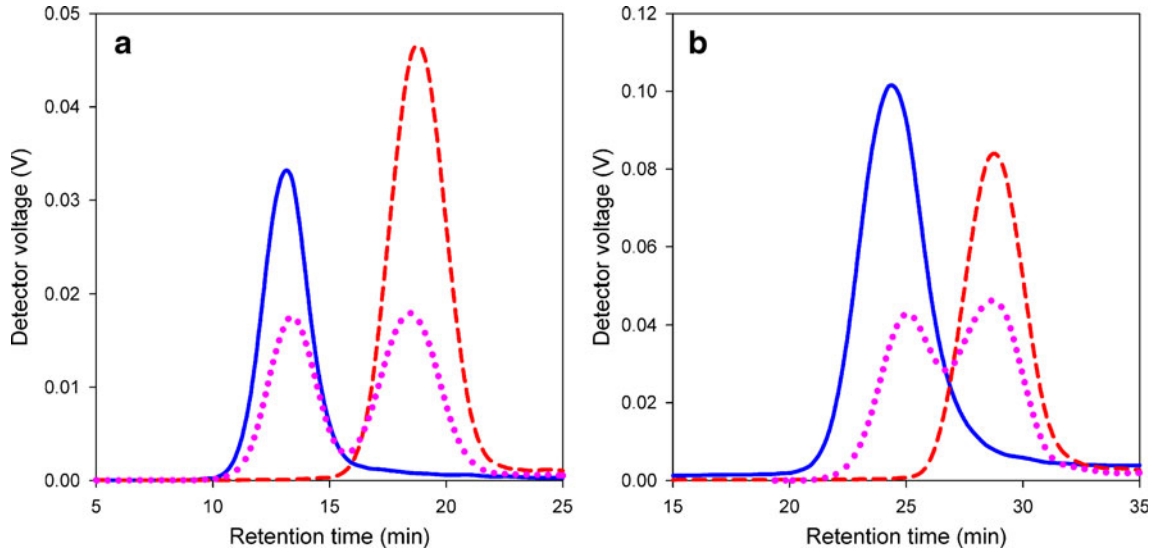

Fig. 9 AFFF fractograms for unconjugated GNPs, GNP-PEG, and their mixtures in 0.02% NaN_3 mobile phase. **a** GNP30, Program C; **b** GNP60, Program D; 90° MALS (LS) trace: (*solid line*) unconjugated GNP; (*dashed line*) GNP-PEG; (*dotted line*) mixture of unconjugated GNP and GNP-PEG

48.1±1.1 and 75.3±2.3 nm, respectively. These values are consistent with, but slightly lower than, the batch-mode DLS results reported above. This is to be expected, since the on-line DLS measurements are obtained across the central portion of the eluting peak where the signal-to-noise level is sufficiently high, excluding any trace quantities of aggregates from the analysis. By contrast, the batch DLS measurements will be influenced by the presence of trace amounts of small aggregates, which skew the result toward larger sizes. Results for the mixtures of conjugated and unconjugated GNPs (dotted lines in Fig. 9) show that the fractions are reasonably well separated, particularly in the case of nominally 30 nm GNPs where baseline separation is evident. In both cases, it is possible to differentiate and separately analyze the principal components, which is ultimately our goal in this exercise.

Effect of accumulation wall membrane chemistry

RC membranes are hydrophilic. In order to probe the effect of membrane chemistry on the separation process in AFFF, we also evaluated hydrophobic PVDF as a membrane material. We knew from filtration work with citrate GNPs that PVDF membranes exhibit less interaction with particles compared with many other standard membrane materials that tend to strip gold particles from solution. Furthermore, the AFFF tests were conducted with a mobile phase consisting of DI water with no added electrolyte, the goal being to develop a method that did not require additives. Early experiments with DI water using RC membranes were problematic; in many cases, the GNP recovery was low, and the smaller size particles eluted too quickly, frequently overlapping the void peak (see, e.g., Fig. 10a, b). In contrast, initial experiments with PVDF suggested that this membrane material was compatible with GNPs and worked well with respect to GNP retention and recovery in a DI water mobile phase. For example, GNP30 and GNP60 can be satisfactorily analyzed as single components in DI water using PVDF (Fig. 10a, b), whereas GNP30 on an RC membrane is convoluted into the void peak and overlaps significantly with the GNP60 retention range. The corresponding peaks elute more slowly with PVDF compared to RC (for GNP30—5.8 min versus 3.5 min; for GNP60—10.1 min versus 5.7 min) and do not produce a contaminated void peak.

Unfortunately, three limiting issues became evident for the application of PVDF membranes. From a practical standpoint, PVDF membranes of sufficient size are not readily available over a range of MWCO values compared with widely used RC membranes; this reduces flexibility in the implementation of PVDF. Secondly, we found that PVDF membranes become fouled or otherwise degraded relatively quickly with continuous use, leading to poor reproducibility of the retention behavior over time compared with RC. Finally, for reasons not completely understood at this time, PVDF performed poorly with respect to separation of multiple components in a mixture as demonstrated for M3 in Fig. 10c, d. For instance, Program C yielded the best overall fractograms for individual and component mixtures of 10, 30, and 60 nm GNPs in a DI water mobile phase over PVDF. As shown in Fig. 10c, d, retention times (determined from either MALS or UV traces) for individual GNP samples (GNP10, GNP30, GNP60) were 2.7, 6.3, and 11.6 min, respectively. Flow-mode DLS measurements yielded the appropriate size for each GNP sample (13.0±

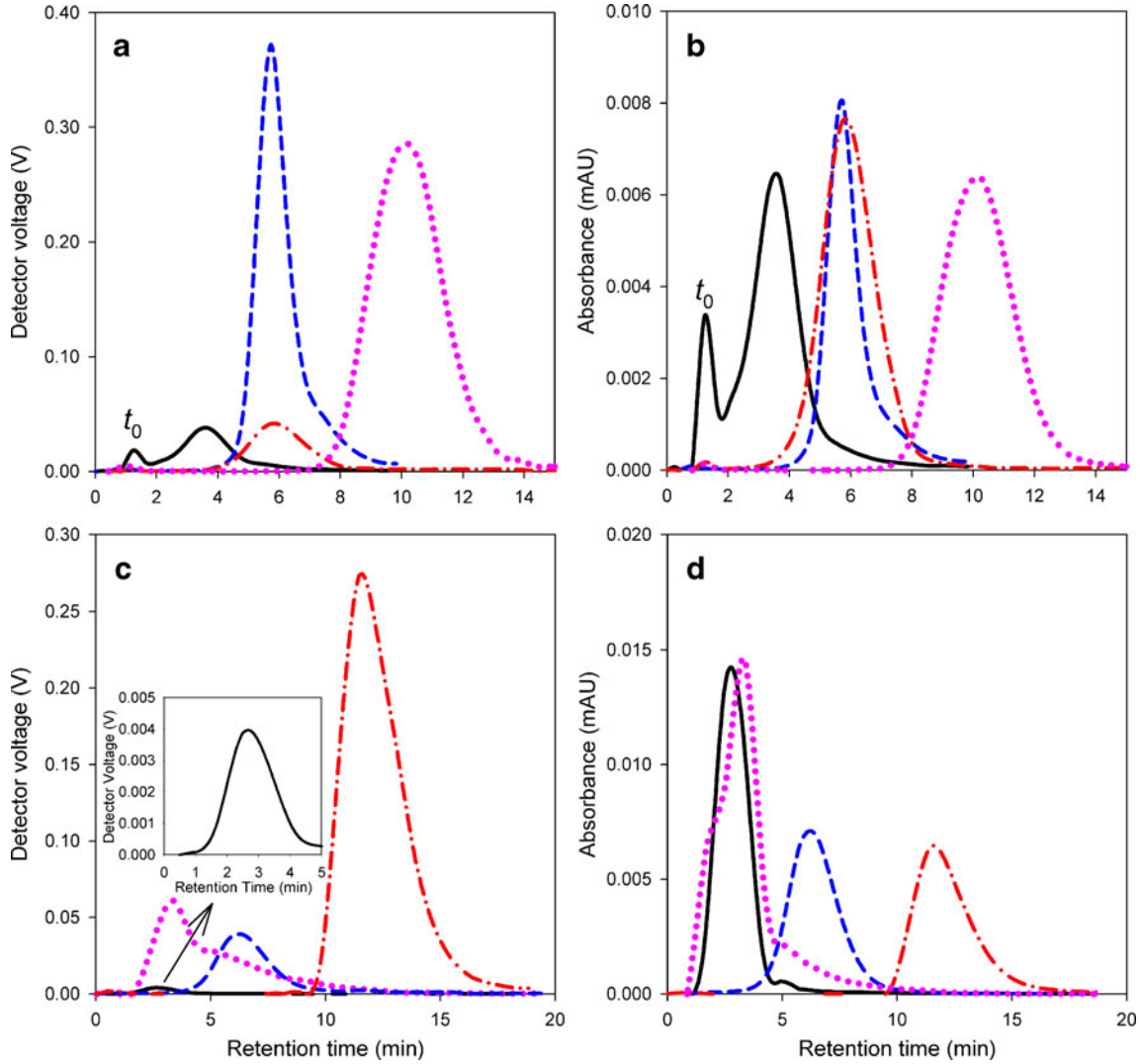

Fig. 10 AFFF fractograms for each individual GNP and their mixture (M3) on PVDF membrane with DI water. **a** 90° MALS (LS) trace, **b** UV trace (Program A): (*solid line*) GNP30 and (*dashed line*) GN P60 on RC membrane; (*dash-dotted line*) GNP30 and (*dotted line*) GNP60 on PVDF membrane. **c** LS trace and **d** UV trace (Program C, PVDF membrane): (*solid line*) GNP10; (*dashed line*) GNP30; (*dash-dotted line*) GNP60; (*dotted line*) M3 mixture

0.6, 29.6±1.0, and 58.5±1.1 nm). But when M3 was analyzed using these same fractionation conditions, the recovery and separation of peaks was extremely poor and clearly unacceptable. The potential advantages of using PVDF (simpler mobile phase with no additives, less interaction with GNPs) are outweighed by the disadvantages as described above.

Conclusions

In this work, the capacity for implementing AFFF in the separation and characterization of citrate-stabilized GNPs and their conjugated analogs was interrogated over a wide range of experimental conditions, with the goal of developing optimized methodology relevant to biomedical applications. Results indicate that the optimum mobile phase compositions with respect to resolution, recovery, and reproducibility are, in descending order: 0.02% NaN_3≥ 0.05% sodium citrate >0.05% SDS≈0.05% SDS+0.02% NaN_3>DI water (all over RC membrane). Notably, a low level ionic strength (up to 10 mmol/L) in the mobile phase improves the GNP retention behavior, produces an appropriate retention ratio value, and yields stable hydrodynamic size measurements. The ionic strength can be obtained by addition of either NaN_3 or sodium citrate. Conversely, eluting with pure DI water was problematic with respect to precision of the GNP characterization measurements. Other surfactant formulations investigated in this study produce measurement artifacts that are deemed unacceptable for GNP analysis. Complex mixtures of GNPs are successfully separated by systematic variation of the channel and cross-

flow rates, as described in detail above. Mixtures containing up to five GNP components (M5) were separated into individual eluting peaks with minimal convolution or overlap. PEG-conjugated GNPs created from the same core particles were analyzed using our AFFF methodology, and mixtures of the PEG-ylated and native (unconjugated) GNPs were baseline resolved using the same program for M5 separation. The use of on-line DLS for size analysis proved to be more robust compared with either off-line DLS batch measurements or determination of hydrodynamic size based on the retention time alone. Although not discussed in the paper, we also examined measurement of the radius of gyration from on-line MALS data, but we did not find the results to be sufficiently robust; nor were they consistent with expectations. This may be related in part to the size range involved in the present work relative to the MALS configuration used and in part due to the novel optical properties of the GNPs themselves. Future efforts will seek to extend the present study to investigate the preparation, separation, and characterization of more complex and novel GNP conjugates.

Acknowledgements The authors wish to thank Dr. Jiwen Zheng of the National Cancer Institute's Nanotechnology Characterization Laboratory (NCI-NCL) for help in generating the PEG-conjugated GNPs used in the study. The cooperation with Dr. Anil K. Patri and Dr. Jeffrey Clogston, also of the NCI-NCL, is gratefully acknowledged.

References

1. Hone DC, Walker PI, Evans-Gowing R, FitzGerald S, Beeby A, Chambrier I, Cook MJ, Russell DA (2002) Langmuir 18:2985–2987
2. Katz E, Willner I (2004) Angew Chem Int Ed 43:6042–6108
3. Kim JH, Lee TR (2004) Chem Mater 16:3647–3651
4. Paciotti GF, Myer L, Weinreich D, Goia D, Pavel N, McLaughlin RE, Tamarkin L (2004) Drug Deliv 11:169–183
5. Shenhar R, Rotello VM (2003) Acc of Chem Res 36:549–561
6. Cheng J-X (2007) Nanomed: Nanotechnol Biol Med 3:345–346
7. Gannon CJ, Patra CR, Bhattacharya R, Mukherjee P, Curley SA (2008) J Nanobiotechnol 6:2–10
8. Huang WC, Tsai PJ, Chen YC (2007) Nanomed 2:777–787
9. Pissuwan D, Valenzuela SM, Killingsworth MC, Xu XD, Cortie MB (2007) J Nanoparticle Res 9:1109–1124
10. El-Sayed IH, Huang XH, El-Sayed MA (2005) Nano Lett 5:829–834
11. Rosi NL, Mirkin CA (2005) Chem Rev 105:1547–1562
12. Storhoff JJ, Mirkin CA (1999) Chem Rev 99:1849–1862
13. Alivisatos AP, Johnsson KP, Peng XG, Wilson TE, Loweth CJ, Bruchez MP, Schultz PG (1996) Nature 382:609–611
14. Mirkin CA, Letsinger RL, Mucic RC, Storhoff JJ (1996) Nature 382:607–609
15. Niemeyer CM (2001) Angew Chem Int Ed 40:4128–4158
16. Storhoff JJ, Mucic RC, Mirkin CA (1997) J Clust Sci 8:179–216
17. Weare WW, Reed SM, Warner MG, Hutchison JE (2000) J Am Chem Soc 122:12890–12891
18. Daniel MC, Astruc D (2004) Chem Rev 104:293–346
19. Eustis S, El-Sayed MA (2006) Chem Soc Rev 35:209–217
20. Busbee BD, Obare SO, Murphy CJ (2003) Adv Mater 15:414–416
21. Martin CR (1994) Science 266:1961–1966
22. Xiong YJ, Washio I, Chen JY, Cai HG, Li ZY, Xia YN (2006) Langmuir 22:8563–8570
23. Aslan K, Lakowicz JR, Geddes CD (2005) Curr Opin Chem Biol 9:538–544
24. He H, Xie C, Ren J (2008) Anal Chem 80:5951–5957
25. Popovtzer R, Agrawal A, Kotov NA, Popovtzer A, Balter J, Carey TE, Kopelman R (2008) Nano Lett 8:4593–4596
26. Giddings JC (1966) Sep Sci 1:123–125
27. Gimbert LJ, Andrew KN, Haygarth PM, Worsfold PJ (2003) Trac-Trends in Anal Chem 22:615–633
28. Kowalkowski T, Buszewski B, Cantado C, Dondi F (2006) Crit Rev Anal Chem 36:129–135
29. Roda B, Zattoni A, Reschiglian P, Moon MH, Mirasoli M, Michelini E, Roda A (2009) Anal Chim Acta 635:132–143
30. Williams SKR, Lee D (2006) J Sep Sci 29:1720–1732
31. Bang DY, Shin DY, Lee S, Moon MH (2007) J Chromatogr A 1147:200–205
32. Jungmann N, Schmidt M, Maskos M (2001) Macromol 34:8347–8353
33. Muthukrishnan S, Plamper F, Mori H, Muller AHE (2005) Macromol 38:10631–10642
34. Petrov PD, Drechsler M, Muller AHE (2009) J Phy Chem B 113:4218–4225
35. Zattoni A, Reschiglian P, Montalti M, Zaccheroni N, Prodi L, Picca RA, Malitesta C (2007) Inorg Chim Acta 360:1063–1071
36. Jackson BP, Ranville JF, Neal AL (2005) Anal Chem 77:1393–1397
37. Lee H, Williams SKR, Wahl KL, Valentine NB (2003) Anal Chem 75:2746–2752
38. Arfvidsson C, Wahlund KG (2003) Anal Biochem 313:76–85
39. Lee H, Williams SKR, Allison SD, Anchordoquy TJ (2001) Anal Chem 73:837–843
40. Giddings JC, Yang FJ, Myers MN (1977) J Virol 21:131–138
41. Thielking H, Kulicke WM (1998) J Microcolumn Sep 10:51–56
42. Chun J, Fagan JA, Hobbie EK, Bauer BJ (2008) Anal Chem 80:2514–2523
43. Moon MH, Kang DJ, Jung JH, Kim JM (2004) J Sep Sci 27:710–717
44. Schimpf M, Caldwell K, Giddings JC (2000) Field flow fractionation handbook. Wiley Interscience, New York
45. Giddings JC (1993) Science 260:1456–1465
46. Ratanathanawongs SK, Giddings JC (1992) Anal Chem 64:6–15
47. Song JH, Kim WS, Lee DW (2003) J Liq Chromatogr Related Technol 26:3003–3035
48. Rameshwar T, Samal S, Lee S, Kim S, Cho J, Kim IS (2006) J Nanosci Nanotechnol 6:2461–2467
49. Oppenheimer LE, Smith GA (1988) Langmuir 4:144–147
50. Anger S, Caldwell K, Niehus H, Muller RH (1999) Pharm Res 16:1743–1747
51. Contado C, Argazzi R (2009) J Chromatogr A 1216:9088–9098
52. Zattoni A, Rambaldi DC, Reschiglian P, Melucci M, Krol S, Garcia AMC, Sanz-Medel A, Roessner D, Johann C (2009) J Chromatogr A 1216:9106–9112
53. Sermsri W, Jarujamrus P, Shiowatana J, Siripinyanond A (2010) Anal Bioanal Chem 396:3079–3085
54. Koppel DE (1972) J Chem Phy 57:4814–4820
55. Kim DH, Moon J, Cho J (2005) J Water Supply Res Technol-Aqua 54:249–259
56. Song JH, Kim W-S, Park YH, Yu EK, Lee DW (1999) Bull Kor Chem Soc 20:1159–1164
57. Mukerjee P, Mysels KJ (1971) Critical Micelle Concentrations of Aqueous Surfactant Systems, National Standard Reference Data Series, No. 36, National Bureau of Standards (US), Washington D.C.
58. van de Hulst HS (1981) Light scattering by small particles. Dover, New York